Spatial and spectral mode selection of heralded single photons from Parametric Down-Conversion in bulk and PPLN

Stefania Castelletto[b], Ivo Pietro Degiovanni[b], Alan Migdall[a], Valentina Schettini[b]
[a]Optical Technology Division,
National Institute of Standards and Technology,Gaithersburg, Maryland 20899-8441,
[b]Istituto Elettrotecnico Nazionale G. Ferraris, Strada delle Cacce 91-10135 Torino (Italy)

ABSTRACT

We describe an experiment in which photon pairs from a parametric down-conversion source are efficiently coupled into single-mode fibers. On detecting one of the photons, the presence of the other photon in its fiber is heralded with a probability of roughly 70% for a pulsed pump configuration in a bulk crystal, and 80% for a CW periodically poled downconverter. The heralding and heralded photons were then analyzed spectrally by a monochromator to determine the effect of the correlation between spectral and spatial mode-matching in the heralding efficiency. Moreover, we theoretically model the heralding efficiency of both bulk and periodically poled crystals. We compare this model with experimental results for these two cases and find good agreement. Analysis of spatial and spectral mode selection, and their mutual correlation, allows controlled engineering of the spectral and spatial emission modes of PDC single photons.

(190.4410)Nonlinear Optics; (270.0270)Quantum optics;(270.4180)Multiphoton processs

1. INTRODUCTION

Parametric down-conversion (PDC) consumes pump photons and produces light with a two-photon field description.[1,2] This two-photon light, which allows one photon to indicate or herald the existence of its twin, is key to applications such as quantum metrology[3] and quantum information.[4–6] In particular, PDC allows the measurement of one photon to effectively prepare its twin in a well defined state,[7] thus creating a single-photon source. The prepared state will be pure only if we project the first PDC photon (called also the *heralding* photon) into a single mode. To optimize this process of collection into a single mode, it is crucial to properly define and measure the efficiency of that preparation. For many quantum information processing applications[5] this single-mode preparation and collection is particularly important.

Toward this goal previous work has defined an important experimental parameter in such a single-photon source - the heralding efficiency, or the mode preparation efficiency, χ_P.[8] This is the efficiency of preparing a photon in the heralded channel in a definite spectral and spatial mode, by specific mode selection of the heralding or trigger arm. It is found from the raw detection efficiency (coincidence / single counts), and the detection losses in the *heralded* channel. In other words, given the biphoton state with its correlations, the *heralding* channel, with its spectral and spatial definition, projects the *heralded* photon into a definite spectral and spatial mode.

Bulk and periodically poled crystal-based PDC sources have been shown to be feasible for Quantum Information (QI) applications. For high efficiency of pair production, and emission at the telecom wavelength, the use of periodically poled crystals is now becoming common.[9] A periodically poled material allows higher PDC production efficiency via noncritical *quasiphase matching*(QPM). By selection of the poling period and operational temperature these crystals can be tailored to many applications. While QI applications certainly benefit from higher pump conversion efficiency, it is not clear that other characteristics of the periodically poled crystals are compatible with these applications. Specifically, the level of uncorrelated background fluorescence (due to the color center formation in bulk periodic poled structure) may limit the uncertainties that can be achieved, particularly if this background light is comparable in intensity with the one of the PDC.

Further author information: (Send correspondence to Stefania Castelletto)
E-mail: castelle@ien.it, Telephone: 0039 011 3919223

Quantum Communications and Quantum Imaging III, edited by Ronald E. Meyers, Yanhua Shih,
Proc. of SPIE Vol. 5893 589315 (2005)

In addition to the advent of new crystal types, pulse-pumping of the crystal is now common.[10–12] With this change, narrow-band spectral filtering must be considered for temporal mode definition, and efficient coupling of the photons into single-mode fibers.

In this paper we present a theoretical analysis of the spectral and spatial PDC emission from both a bulk and a QPM periodically poled structure, and its impact on the coupling efficiency into single-mode fibers (SMF). Our analysis considers two experimental configurations: a pulse-pumped downconverter with a bulk crystal and a CW-pumped periodically poled downconverter. Central to this work is our continuing effort to explore the effect of the pulsed versus CW pump on the PDC spectral emission. Others efforts in this direction are pursued.[13]

2. THEORETICAL MODEL FOR BULK AND PERIODICALLY POLED CRYSTALS WITH A PULSED PUMP

Here we use a theoretical approach to predict the spectral and spatial correlations of the PDC photon pair to allow the mode preparation efficiency to be maximized for the cases of a bulk nonlinear crystal and a periodically poled crystal. Our calculations, use the spatial mode preparation results obtained elsewhere.[8,14] Because this derivation is taken only to first order to make the problem tractable, correlations between the spatial and spectral portions of the phasematching function are left out. To correct for this, an adhoc term is added. We deduce the fiber spectral selection from the slope of the PDC curve $\theta_o(\lambda_{s,i})$ (with no phase mismatch), while we get the width due to the longitudinal wavevector mismatch calculated to first order.

We note[15] that the biphoton state can be written in terms of the classical pump $E_p(x,y,z,t)$ field and the signal and idler photons' negative frequency-portion of the electric field operators, $\widehat{E}^{(-)}_{s,i}(x,y,z,t)$, as

$$|\psi\rangle = \int_{-\infty}^{\infty} \mathrm{d}t \int_V \mathrm{d}x\ \mathrm{d}y\ \mathrm{d}z\ E_p(x,y,z,t)\widehat{E}^{(-)}_s(x,y,z,t)\widehat{E}^{(-)}_i(x,y,z,t)\chi^{(2)}(z)|0_{\mathbf{k}_\mathrm{s},\omega_\mathrm{s}}\rangle|0_{\mathbf{k}_\mathrm{i},\omega_\mathrm{i}}\rangle. \tag{1}$$

$\chi^{(2)}(z) = \chi^{(2)}$ is the nonlinear susceptibility for bulk crystal and $\chi^2(z) = \chi^2 \exp(-i2\pi/\Lambda z)$, for periodically poled with period Λ. Here we replace the classical pump field with its transverse and spectral Fourier transform, according to

$$E_p(x,y,z,t) = \int \mathrm{d}^3k_p \mathrm{d}\omega_p \widetilde{E}_{q_p}(\mathbf{q}_p)\widetilde{E}_{\nu_p}(\omega_p)e^{i\mathbf{k}_p\cdot\mathbf{r}-i\omega_p t}, \tag{2}$$

rewriting the two-photon state at the output surface of a PDC crystal oriented with its face perpendicular to the z-axis as obtained in ref.[14]

$$|\psi\rangle = \int \mathrm{d}^3k_\mathrm{s}\mathrm{d}\omega_\mathrm{s}\mathrm{d}^3k_\mathrm{i}\mathrm{d}\omega_\mathrm{i}\widetilde{A}_{12}(\mathbf{k}_\mathrm{s},\mathbf{k}_\mathrm{i},\omega_\mathrm{i},\omega_\mathrm{s})|1_{\mathbf{k}_\mathrm{s},\omega_\mathrm{s}}\rangle|1_{\mathbf{k}_\mathrm{i},\omega_\mathrm{i}}\rangle, \tag{3}$$

where

$$\begin{aligned}
\widetilde{A}_{12}(\mathbf{k}_\mathrm{s},\mathbf{k}_\mathrm{i},\omega_\mathrm{i},\omega_\mathrm{s}) \quad \propto \quad & \int \mathrm{d}^3k_\mathrm{p}\mathrm{d}\omega_\mathrm{p}\int_S \mathrm{d}x\mathrm{d}y\int_{-L}^{0}\mathrm{d}z\ \widetilde{E}_{\mathrm{q_p}}(\mathbf{q}_\mathrm{p})\widetilde{E}_{\nu_\mathrm{p}}(\omega_\mathrm{p})\chi^2(z)e^{i(\Delta k_x x+\Delta k_y y+\Delta k_z z)} \\
& \times\delta(\omega_\mathrm{s}+\omega_\mathrm{i}-\omega_\mathrm{p}) \\
& \times\delta\left[k_{p_z}-\sqrt{\left(\frac{n(\Omega_p)\Omega_p}{c}\right)^2-\mathbf{q}_p^2}\right] \\
& \times\delta\left[k_{s_z}-\sqrt{\left(\frac{n(\omega_s)\omega_s}{c}\right)^2-\mathbf{q}_s^2}\right] \\
& \times\delta\left[k_{i_z}-\sqrt{\left(\frac{n(\omega_i)\omega_i}{c}\right)^2-\mathbf{q}_i^2}\right],
\end{aligned} \tag{4}$$

S is the cross sectional area of the crystal illuminated by the pump, and L is the length of the crystal. The subscripts s, i, p indicate the signal, idler, and pump. The pump beam propagates along the z axis. We evaluate $\Delta k_{x,y,z} = (\mathbf{k}_p - \mathbf{k}_s - \mathbf{k}_i)_{x,y,z}$, in terms of the pump, signal, and idler k-vectors. The longitudinal component of the pump k-vector is

$$k_{p_z} = \sqrt{\left(\frac{n(\omega_p)\omega_p}{c}\right)^2 - \mathbf{q}_p^2}, \tag{5}$$

where $\mathbf{q}_p$ is the transverse component of the pump k-vector and c is the speed of light. Analogous expressions give the signal and idler longitudinal components.

$\widetilde{E}_{\nu_p}(\omega_p) = \exp(-\frac{1}{8a^2}(\omega_p - \Omega_p)^2 T_p^2)$, is the pump pulse frequency distribution, where T_p is the temporal width of the pulse at FWHM and $\widetilde{E}_{q_p} = \exp(-\frac{w_p^2 q_p^2}{4})$ is the pump transverse wavevector distribution with w_p being the pump field waist ($a = 2\sqrt{\ln(2)}$ is the conversion factor between the FWHM and the $1/e^2$ radius of the field profile). Both are assumed for simplicity to be Gaussian. We write the wavevector mismatch $\Delta k_{x,y,z}$ terms as

$$\begin{aligned} \Delta k_x &= q_{p_x} - q_{s_x} - q_{i_x} \\ \Delta k_y &= q_{p_y} - q_{s_y}\cos\theta_s - q_{i_y}\cos\theta_i \\ \Delta k_z &= D_{pi}\nu_p + D_{is}\nu_s + (\mathcal{N}_p - \mathcal{N}_s\cos\theta_s - \mathcal{N}_i\cos\theta_i)\frac{q_{p_y}}{K_p} + \sin\theta_s q_{s_y} + \sin\theta_i q_{i_y}, \end{aligned} \tag{6}$$

where $\theta_{i,s}$ are the emission angles of the idler and signal photons, and $K_{i,s,p} = n_{i,s,p}(\Omega_{i,s,p}, \phi)\Omega_{i,s,p}/c$ describe the directions of the central intensities of the wavevectors. $\theta_{i,s}$ are obtained from the transverse and longitudinal perfect phase-matching condition for the central emissions and wavelengths, given for bulk respectively by $K_i \sin\theta_i = K_s \sin\theta_s$ and $K_p = K_s\cos\theta_s + K_i\cos\theta_i$, while for periodically poled $K_p = K_s\cos\theta_s + K_i\cos\theta_i + \frac{2\pi}{\Lambda}$, namely the longitudinal perfect phase-matching given by the period Λ. The terms, $\mathcal{N}_p = \frac{\Omega_p}{c}\frac{\mathrm{d}n_p(\Omega_p,\phi)}{\mathrm{d}\phi}|_{\phi_o}$ and $\mathcal{N}_{s,i} = \frac{\Omega_{s,i}}{c}\frac{\mathrm{d}n_{s,i}(\Omega_{s,i},\phi)}{\mathrm{d}\phi}|_{\phi_o}$ account for the effects of the refractive indexes of the pump and the signal due to the pump angular spread, which is responsible for a small deviation from the phase-matching angle ϕ_o.

The other terms are defined as $D_{is} = D_i(\cos\theta_i - \sin\theta_i\tan\theta_i) - D_s(\cos\theta_s + \sin\theta_s\tan\theta_s)$, $D_{pi} = -D_i(\cos\theta_i + \sin\theta_i\tan\theta_i) + D_p$, and $\nu_{i,s,p} = \omega_{\mathrm{i,s,p}} - \Omega_{\mathrm{i,s,p}}$ with $D_{i,s}\frac{\mathrm{d}n_{\mathrm{i,s}}(\omega_{\mathrm{i}},\phi)\omega_{\mathrm{i,s}}/c}{\mathrm{d}\omega_{\mathrm{i,s}}}|_{\Omega_{\mathrm{i,s}}}$, $D_p = \frac{\mathrm{d}n_{\mathrm{p}}(\omega_{\mathrm{p}},\phi)\omega_{\mathrm{p}}/c}{\mathrm{d}\omega_{\mathrm{p}}}|_{\Omega_{\mathrm{p}}}$, $\nu_p = \nu_i + \nu_s$. Note that $\mathcal{N}_{s,i} = 0$ for Type I phase-matching in bulk crystal. In the periodically poled case there is no birefringence so $\mathcal{N}_{s,i} = \mathcal{N}_p = 0$, because we have non critical phase-matching, $\phi_o = \pi/2$. Assuming S infinite, we integrate over x and y, giving $\Delta k_x = \Delta k_y = 0$. To obtain the biphoton field in the transverse spatial and time variables, we take the Fourier transforms on the q and ν variables and integrate over z,

$$\begin{aligned} A_{12}(\rho_1, \rho_2, t, \tau) \quad \propto \quad & E_{\nu_p}(\frac{\tau - t + 2\tau D_{pi}/D_{is}}{2}) E_{q_p}(x_1, y_1 - \frac{\mathcal{N}_{p,s}\tau}{K_p D_{is}}) \\ & \delta(x_1 - x_2) \times \delta(y_1 - y_2 + \frac{\alpha_s \tau}{D_{is}}) \Pi_{D_{is}L}(\tau), \end{aligned} \tag{7}$$

where $\mathcal{N}_{p,s} = -\mathcal{N}_s(\cos\theta_s + \sin\theta_s\tan\theta_i) + \mathcal{N}_p - K_p\tan\theta_i$, $\alpha_s = -\cos\theta_s\tan\theta_i + \sin\theta_s$, $\tau = t_1 - t_2$, $t = t_1 + t_2$ and $\Pi_{D_{is}L}(\tau) = 1$ for $0 \le \tau \le D_{is}L$ and 0 elsewhere. t_1 and t_2 are the times when the two photons are generated at the longitudinal positions z_1=z_2=0, at the crystal output surface.

To obtain Eq. (7) we made some approximations. First, we assumed that the pump, signal, and idler have narrow transverse angular distributions, so we can use the paraxial approximation. We also rewrite the longitudinal k-vector components by expanding the index of refraction $n_{p,s,i}(\omega_{p,s,i}, \phi)$ around the central frequencies ($\Omega_{s,i}$), and around the phase-matching angle ϕ_o. This approximation holds only in cases where the considered field is an extraordinary wave (this of course depends on the type of phase-matching adopted, either type I or type II). In all cases, we limited our calculation to the first perturbative order. We also assume small non-collinearity and small walk-off angles. $E_{\nu_p}(\frac{\tau - t + 2\tau D_{pi}/D_{is}}{2})$ is the time Fourier transform of the pump spectral distribution $\widetilde{E}_{\nu_p}(\nu_p)$ and $E_{q_p}(x_1, y_1 - \frac{\mathcal{N}_{s,p}\tau}{K_p D_{is}})$ is similarly the Fourier transform of pump transverse momentum distribution $\widetilde{E}_{q_p}$. To calculate the coincidence rates measured by two single mode fibers in the signal and idler

arms, we assume first that the guided transverse spatial modes are Gaussian fields propagated back from the fibers through the lenses and crystal output surface, and are defined by

$$\varphi_j^*(x_j, y_j) = \sqrt{\frac{2}{\pi}} \frac{1}{w_{o,j}} \exp\left[-\frac{(x_j^2 + y_j^2)}{w_{o,j}^2}\right], \tag{8}$$

with $j = 1, 2$. The imaging optic L_j is arranged to place the collection beam waist, $w_{o,j}, j = 1, 2$ are the fiber waists at the crystal with the lens clear apertures are greater than $\Delta\theta_{1,2} d_{1,2}$. We work in the perfect imaging configuration where the gaussian field guided by a fiber is magnified by the lens and if $w_{f,j}$ is the fiber waist at the fiber exit tip, the beam waist at the crystal is $w_{o,j} = M_j w_{f,j}$.

The resulting time dependent biphoton field is calculated by integrating over the transverse spatial variables according to

$$\mathcal{A}_{12}(t, \tau) = \int \mathrm{d}\rho_1 \mathrm{d}\rho_{\mathbf{2}} A_{12}(\rho_1, \rho_2, t, \tau) \varphi_1^*(\rho_1) \varphi_2^*(\rho_2). \tag{9}$$

Here we have to consider that either we spectrally select the PDC photons by an interference filter and/or by single spatial mode collection, acting also as a spectral filter. We eventually identify a single mode fiber as a spectral filter with a gaussian spectral distribution given by $\widetilde{I}_{\nu_{s,i}}(\nu_{s,i}) = e^{(-\frac{a^2}{\Delta_{1,2}^2}\nu_{s,i}^2)}$ with $\Delta_{1,2}$ being the FWHM of the spectral distribution. The geometric collection selected spectral width component at the FWHM by the fiber (see fig.(1)), $\Delta_{1,2}$, is given by the FWHM angular collection $\Delta\theta_{1,2} = a\frac{\lambda}{\pi w_{o,1,2}}$ and the spectral/angular spread of the PDC, $\theta_o(\lambda_{s,i})$, around the central wavelength $\lambda_{i,s}$. Therefore by Fourier transforming the spectral filter distributions as $I_{\nu_s}(t - t' + \tau - \tau')$ and $I_{\nu_i}(t - t' - \tau + \tau')$ the coincidence rate is

$$C_{12} = \int \mathrm{d}t\mathrm{d}t'\mathrm{d}\tau\mathrm{d}\tau'_{12}(t, \tau) \mathcal{A}_{12}(t, \tau) \mathcal{A}_{12}^*(t', \tau') I_{\nu_s}(t - t' + \tau - \tau') I_{\nu_i}(t - t' - \tau + \tau'). \tag{10}$$

Singles rates are calculated with only one fiber-defined spatial mode, i.e. first by calculating

$$\mathrm{A}_{12}(t, \tau, \rho_2) = \int \mathrm{d}\rho_1 A_{12}(\rho_1, \rho_2, t, \tau) \varphi_1^*(\rho_1) \tag{11}$$

and then integrating over the spectral filter as

$$C_1 = \int \mathrm{d}\rho_2 \mathrm{d}t\mathrm{d}t'\mathrm{d}\tau\mathrm{d}\tau' \mathrm{A}_{12}(t, \tau, \rho_2) \mathrm{A}_{12}^*(t', \tau', \rho_2) I_{\nu_s}(t - t' + \tau - \tau'). \tag{12}$$

The mode preparation efficiency is finally

$$\chi_{\mathrm{P}} = \frac{C_{12}}{C_1}. \tag{13}$$

For the case where arm 1 is the heralding channel the general result is

$$\chi_{\mathrm{P}} = \frac{4\ T_p\ w_{o,1}^2 w_{o,2}^2 w_p^2\ (w_{o,1}^2 + w_p^2)\Delta_2}{(w_{o,2}^2 w_p^2 + w_{o,1}^2(w_{o,2}^2 + w_p^2))^2 \sqrt{8a^6 + T_p^2(\Delta_1^2 + \Delta_2^2)}} \frac{f(c_1, c_2)}{f(s_1, s_2)} \tag{14}$$

where

$$f(p, q) = \frac{\int_0^1 \mathrm{d}x\ e^{-px^2 + \frac{q^2 x^2}{4p}} (\mathrm{Erf}[\frac{qx}{2\sqrt{p}}] - \mathrm{Erf}[\frac{-2p + qx}{2\sqrt{p}}])}{\sqrt{p}} \tag{15}$$

The parameters are here explicitly written for a generic case:

$$c_1 = -\frac{L^2}{4a^2} \left\{ \begin{array}{c} -\frac{4\ a^2 \mathcal{N}_{s,p}^2 (w_{o,1}^2 + w_{o,2}^2) + 8\ a^2 K_p \mathcal{N}_{s,p} w_{o,1}^2 \alpha_s + K_p^2 (w_p^2 (4\ a^2 \alpha_s^2 + D_{is}^2 w_{o,2}^2 (\Delta_1^2 + \Delta_2^2)) + K_p^2 w_p^2 (4\ a^2 \alpha_s^2 + D_{is}^2 (w_{o,2}^2 + w_p^2)(\Delta_1^2 + \Delta_2^2))}{K_p^2 [w_{o,2}^2 w_p^2 + w_{o,1}^2 (w_p^2 + w_{o,2}^2)]} + \\ \frac{-64\ a^6 D_{pi} D_{is} \Delta_1^2 - 32\ a^6 D_{p,i} (\Delta_1^2 + \Delta_2^2) + D_{is}^2 (8\ a^6 \Delta_2^2 + T_p^2 \Delta_i^4 - 2(12\ a^6 + T_p^2 \Delta_1^2 + T_p^2 \Delta_1^4))}{8\ a^6 + T_p^2 (\Delta_1^2 + \Delta_2^2)} \end{array} \right\}$$

$$
\begin{aligned}
c_2 &= \frac{2L^2\{8a^6D_{pi}^2\Delta_2^2+[8\ a^6(D_{is}+D_{pi})^2+D_{is}^2T_p^2\Delta_2^2]\Delta_1^2\}}{a^2[8\ a^6+T_p^2(\Delta_1^2+\Delta_2^2)]}\\
s_1 &= \frac{L^2}{2}\left[\frac{16\ a^4D_{pi}^2}{T_p^2}+\frac{\mathcal{N}_{s,p}^2}{K_p^2}\left(\frac{1}{w_p^2+w_{o,1}^2}+\frac{1}{w_p^2}\right)+\frac{2\mathcal{N}_{s,p}\alpha_s}{K_pw_p^2}+\alpha_s^2\left(\frac{1}{w_{o,1}^2}+\frac{1}{w_p^2}\right)+\frac{2D_{is}^2\Delta_1^2}{a^2}\right]\\
s_2 &= L^2\left\{\frac{16\ a^4D_{pi}^2}{T_p^2}+\frac{[\mathcal{N}_{s,p}w_{o,1}^2+K_p(w_{o,1}^2+w_p^2)\alpha_s]^2}{K_p^2w_{o,1}^2w_p^2(w_{o,1}^2+w_p^2)}+\frac{2D_{is}^2\Delta_1^2}{a^2}\right\}.
\end{aligned}
\tag{16}
$$

The coincidence spectrum is determined by taking only the Fourier transform of the transverse spatial variables in Eq.(3), obtaining

$$
\begin{aligned}
\mathbf{A}_{12}(\rho_1,\rho_2,\nu_s,\nu_i) \propto\ & \widetilde{E}_{\nu_p}(\nu_s+\nu_i)E_{q_p}(x_1,y_1+(y_1-y_2)\frac{\mathcal{N}_{s,p}}{K_p\alpha_s})\times\\
& \exp[\frac{\mathrm{I}(y_1-y_2)(\nu_sD_{is}+(\nu_i+\nu_s)D_{pi})}{\alpha_s}]\ \delta(x_1-x_2)\Pi_{-L}(\frac{y_1-y_2}{\alpha_s}).
\end{aligned}
$$

Therefore the resulting frequency dependent biphoton field is calculated by integrating over the transverse spatial variables according to

$$
\mathcal{A}_{12}(\nu_s,\nu_i)=\int \mathrm{d}\rho_1\mathrm{d}\rho_{\mathbf{2}}\mathbf{A}_{12}(\rho_1,\rho_2,\nu_s,\nu_i)\varphi_1^*(\rho_1)\varphi_2^*(\rho_2). \tag{17}
$$

The coincidence spectrum is

$$
C_{12}(\nu_i)=\int \mathrm{d}\nu_s|\mathcal{A}_{12}(\nu_s,\nu_i)|^2\widetilde{I}_{\nu_i}(\nu_i)\widetilde{I}_{\nu_s}(\nu_s)=\int \mathrm{d}\nu_s\mathcal{C}_{12}(\nu_i,\nu_s). \tag{18}
$$

We explicitly write $\mathcal{C}_{12}(\nu_i,\nu_s)$ as

$$
\begin{aligned}
\mathcal{C}_{12}(\nu_i,\nu_s) \propto\ & \left|\widetilde{E}_{\nu_p}\left[(\nu_s+\nu_i)\left(1+\frac{64\ a^4\zeta^2[\nu_sD_{is}+(\nu_i+\nu_s)D_{pi}]^2}{T_p^2(\nu_i+\nu_s)^2}\right)^{1/2}\right]\right|^2\widetilde{I}_{\nu_i}(\nu_i)\widetilde{I}_{\nu_s}(\nu_s) \qquad (19)\\
& \left|\mathrm{Erf}\left[-\frac{L}{2\zeta}-\mathrm{i}\zeta[\nu_sD_{is}+(\nu_i+\nu_s)D_{pi}]\right]+\mathrm{Erf}\left[\mathrm{i}\zeta[\nu_sD_{is}+(\nu_i+\nu_s)D_{pi}]\right]\right|^2
\end{aligned}
$$

where

$$
\zeta=\frac{K_p\sqrt{w_{o,2}^2w_p^2+w_{o,1}^2(w_{o,2}^2+w_p^2)}}{2\sqrt{\mathcal{N}_{s,p}^2(w_{o,1}^2+w_{o,2}^2)+2K_p\mathcal{N}_{s,p}w_{o,1}^2\alpha_s+K_p^2(w_{o,1}^2+w_p^2)\alpha_s^2}}. \tag{20}
$$

From Eq.(19) we deduce that the interplay between the spectral components $\nu_{i,s}$ and the transverse parameters $w_{o,p}$ is quantified by ζ, contained in the Erf terms, which is relevant to both the pump pulse envelope and the pump transverse distribution. Note that while for w_p large, the term $\widetilde{E}_{\nu_p}[(\nu_s+\nu_i)(1+\frac{64\ a^4\zeta^2[\nu_sD_{is}+(\nu_i+\nu_s)D_{pi}]}{T_p^2(\nu_i+\nu_s)^2})^{1/2}]$ contributes to a widened coincidence spectrum, the Erf terms instead reduce the overall coincidence spectrum width.

3. THEORETICAL MODEL FOR BULK AND PPLN CRYSTAL WITH A CW PUMP

The same approach can be used for a CW pump. The final result can be obtained from the biphoton field as

$$\begin{aligned} A_{12}^{CW}(\rho_1,\rho_2,\tau) &\propto E_{q_p}(x_1, y_1 - \frac{\mathcal{N}_{p,s}\tau}{K_p D_{is}}) \\ &\quad \delta(x_1 - x_2) \times \delta(y_1 - y_2 + \frac{\alpha_s \tau}{D_{is}}) \Pi_{D_{is}L}(\tau). \end{aligned} \tag{21}$$

After the spatial integrations

$$\mathcal{A}_{12}^{CW}(\tau) = \int \mathrm{d}\rho_1 \rho_2 A_{12}^{CW}(\rho_1,\rho_2,\tau)\varphi_1^*(\rho_1)\varphi_2^*(\rho_2), \tag{22}$$

and

$$\mathrm{A}_{12}^{CW}(\tau,\rho_2) = \int \mathrm{d}\rho_1 A_{12}^{CW}(\rho_1,\rho_2,\tau)\varphi_1^*(\rho_1), \tag{23}$$

we obtain

$$C_{12} = \int \mathrm{d}t\mathrm{d}t'\mathrm{d}\tau\mathrm{d}\tau' \mathcal{A}_{12}{}^{CW}(\tau)\mathcal{A}_{12}^{*}{}^{CW}(\tau') I_{\nu_s}(t - t' + \tau - \tau') I_{\nu_i}(t - t' - \tau + \tau'), \tag{24}$$

and singles rates

$$C_1 = \int \mathrm{d}\rho_2 \mathrm{d}t\mathrm{d}t'\mathrm{d}\tau\mathrm{d}\tau' \mathrm{A}_{12}^{CW}(\tau,\rho_2)\mathrm{A}_{12}^{CW\,*}(\tau',\rho_2)\varphi_1^* I_{\nu_s}(t - t' + \tau - \tau'). \tag{25}$$

The mode preparation efficiency is

$$\chi_{\mathrm{P}} = \frac{4\ w_{o,1}^2 w_{o,2}^2 w_p^2\ (w_{o,1}^2 + w_p^2)\Delta_2}{(w_{o,2}^2 w_p^2 + w_{o,1}^2(w_{o,2}^2 + w_p^2))^2 \sqrt{(\Delta_1^2 + \Delta_2^2)}} \frac{f(c_1,c_2)}{f(s_1,s_2)}. \tag{26}$$

The parameters are calculated from Eq.(16) simply as $T_p \longrightarrow \infty$.

The biphoton field is

$$\begin{aligned} A_{12}(\rho_1,\rho_2,\nu_s,\nu_i) &\propto E_{q_p}(x_1, y_1 + (y_1 - y_2)\frac{\mathcal{N}_{s,p}}{K_p \alpha_s}) \times \\ &\quad \exp[\frac{\mathrm{I}(y_1 - y_2)(\nu_s D_{is} + (\nu_i + \nu_s)D_{pi})}{\alpha_s}]\ \delta(x_1 - x_2)\Pi_{-L}(\frac{y_1 - y_2}{\alpha_s})\ \delta(\nu_i + \nu_s). \end{aligned}$$

The coincidence spectrum is in this case

$$\begin{aligned} \mathcal{C}_{12}(\nu_i,\nu_s) &\propto \exp[-2\zeta^2[\nu_s D_{is} + (\nu_i + \nu_s)D_{pi}]^2]\widetilde{I}_{\nu_i}(\nu_i)\widetilde{I}_{\nu_s}(\nu_s)\ \delta(\nu_i + \nu_s) \\ &\quad \left|\mathrm{Erf}\left[-\frac{L}{2\zeta} - \mathrm{i}\zeta[\nu_s D_{is} + (\nu_i + \nu_s)D_{pi}]\right] + \mathrm{Erf}\left[\mathrm{i}\zeta[\nu_s D_{is} + (\nu_i + \nu_s)D_{pi}]\right]\right|^2 \end{aligned} \tag{27}$$

4. PULSED PUMP EXPERIMENTAL SETUP

An overview of the source is shown in Figure 1. The idea is to select the *heralding* photon from a single spatial mode, and collect the *heralded* photon in a single spatial mode, where each mode is defined by a single-mode fiber(SMF). In both channels we define our single modes by backward propagating and imaging the single-mode fibers onto the PDC crystal as shown in Fig. (1). The goal is to match and overlap the single-mode beams in the crystal spatially, while considering the extra divergence due to the PDC phase-matching conditions over the wavelength range of interest.

In this experiment, the PDC source was a 5 mm long $\mathrm{LiI0_3}$ crystal pumped by frequency-doubled Ti-Sapphire laser pulses at a repetition rate of 76 MHz and a wavelength of 394.5 nm, with a duration of approximately 150

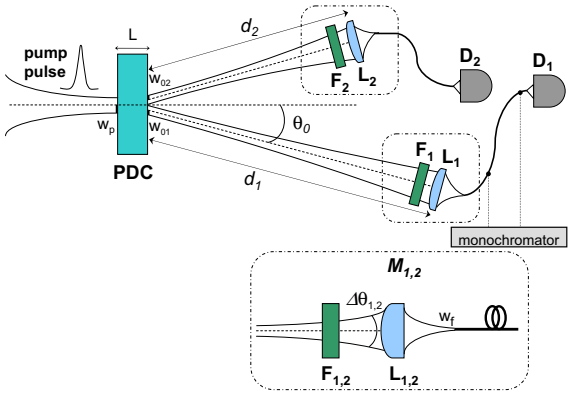

Figure 1. Setup used to herald single-photons from pulsed parametric down-conversion (PDC). Filters $F_{1,2}$, either cut-off or interference and various lenses $L_{1,2}$ are used. Distances $d_{1,2}$ were chosen for practical reasons, and the direction 1 was the heralding channel. A monochromator was inserted in the heralding channel fiber link to measure coincidence spectral distribution

fs. The $LiI0_3$ crystal was oriented to produce photon pairs at 789-791 nm at an external cone angle of θ_0=3.4°, with a phase-matching internal angle of ϕ_o=44.15°. In this case the theory in Section 1 is modified for the almost degenerate case and type I, namely $D_{is} \approx 0$ and $\alpha_s \approx 0$. Two small diametrically opposed regions of the emitted cone were coupled at two different distances from the crystal d_1=53 cm and d_2=38 cm, into single-mode fibers. Lenses (L_1 and L_2) are aspheric (details are given in Table I) The pump beam was focused at the crystal with a beam waist w_p of 260 μm.

Table 1. Details of lens configurations for coupling fiber mode diameter of 4.2 μm, and M are magnifications.

L_1 @ d_1	$w_{0,1}$ (μm)	M_1	Δ_1 (nm)	$\Delta\theta_1$ (°)	L_2 @ d_2	$w_{0,2}$ (μm)	M_2	Δ_2 (nm)	$\Delta\theta_2$ (°)	χ_p(theory) (%)	χ_p(expt.) (%)
f=8mm	137	65	29	0.12	f=8mm	97	47	40	0.17	86	70

4.1. Experimental results

We now analyze the coincidence spectrum for the specific optical setup used. A Gaussian beam analysis yields FWHM angular spreads of $\Delta\theta_{1,2}$ =0.12, 0.17° for the photon field according to the lens configuration (refer to Table I), corresponding to a SMF spectral bandwidth $\Delta_{1,2} = 29, 40$ nm.

We used a spectral filter F_1 centered at 789.3 nm with FWHM of 5 nm in the heralding channel (trigger) to obtain the best heralding efficiency. A cut-off filter F_2 was used to reduce the background light in the heralded arm. A monochromator with 1 nm resolution was used for the coincidence spectral scan. F_1 reduced the bandwidth of the accepted trigger photons along with the bandwidth of the heralded photons. In this way, the choice of F_1 can be used to tailor the spectral properties of the heralded photons. Figure 2 shows the effects of restricting the heralding photon bandwidth to 5 nm (centered at 789 nm) versus the case where only the raw bandwidths (namely the heralding and heralded bandwidths) selected by the two fibers are used. It is clear that, even in the absence of the interference filter, the overall coincidence bandwidth (heralded bandwidth) is reduced with respect to the single fiber selection spectral bandwidths, $\Delta_{1,2}$, and this is the signature that even in this case we have an entanglement between transverse and spectral components. We measured heralded bandwidth of ????? nm. With the 5 nm interference filter inserted, the final bandwidth is about 4 nm. The theoretical predictions match quite well with the experimental results.

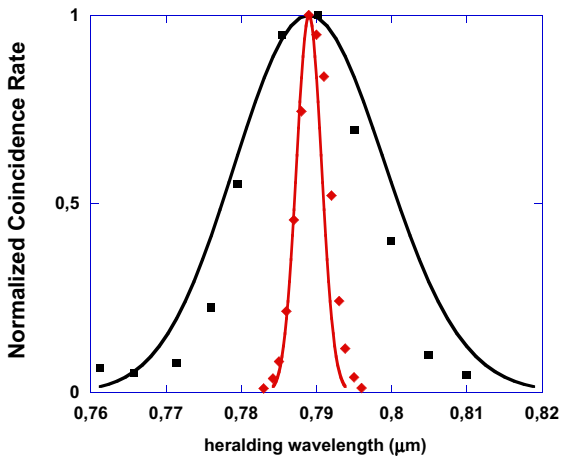

Figure 2. Spectral scan of the normalized coincidence rates performed with a monochromator in the heralding fiber path. Solid lines are theoretical curves of Eq.(18). The narrower scans were taken with a 5 nm FWHM interference filter on the heralding arm.

These results show a narrow coincidence spectral bandwidth profile with respect to the estimated single channel bandwidth selection ($\Delta_{1,2}$), because the heralding channel bandwidth and the correlation dominate. Moreover to restrict the coincidence bandwidth, a narrow filter on the heralding arm is necessary. This means that a spatial mode defined by the SMF contains a wider spectral mode.

To determine the difference between the spatial mode and the spectral mode selection operated by the SMFs, we measured the mode preparation efficiency and the single counts of the heralded channel versus an iris aperture at the collecting lens. We observed that the heralding efficiency, and the single heralded counts level off almost the same iris aperture, corresponding to a measured waist of the mode at the lens of roughly 1.1 mm, which is in agreement with a gaussian mode of 2.1 μm waist at the fiber tip back propagated through a f=8 mm lens, in a perfect imaging configuration.

We made a coincidence spectral scan for 3 fixed iris apertures in Fig.3.

From the measured spectral scan, we see that the spectral width is independent of iris diameter down to at least 1 mm, which is to be expected as the "spectral mode waist" was estimated to be 0.7 mm ($1/\sqrt{2}$ of the spatial waist). In other words, in this case the fiber is just a spatial filter, providing an intensity profile selection. However to obtain the highest efficiency we must match the spatial modes, which are spatially wider than the spectral modes selected by the fiber. In contrast, spectral modes do not have to be matched. This is more evident in the pulsed case than in the CW case. In fact, the use of matched filters (F_1 and F_2) in pulsed PDC will cause an undesirable loss of heralded photons. The heralded bandwidth needs to be significantly wider than that of the trigger-photon filter F_1.

The experimental mode preparation efficiency was obtained by measuring the raw detection efficiency, χ_D, of heralded photons, and then correcting for the losses in the heralded-photon arm, τ_{opt}, and SMF-lens trans-

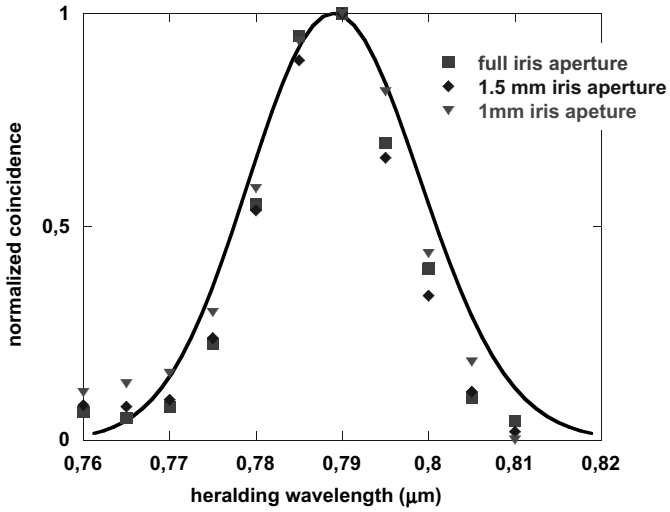

Figure 3. Spectral scan coincidence for various iris diameters on the heralded arm. Data (squares for the full aperture, diamonds at 1.5 mm iris diameter, and down triangles for 1 mm iris diameter) are compared to the theoretical prediction.

mittance, $\tau_{SMP-lens}$,

$$\chi_p = (\eta_{det} \cdot \tau_{opt} \cdot \tau_{SMF-lens})^{-1} \times \chi_D. \tag{28}$$

$\chi_{\rm D}$ was simply defined as the coincidence counting rate, R_c, divided by the trigger photon detection rate, R_1, $\chi_{\rm D} = R_c/R_1$.

Loss in the heralded-photon path of Figure 1 was due to a calibrated detector D_2 with quantum efficiency of η_{det}=53.7% at 790 nm,[16] a measured F_2 transmittance of 91% for the cut-off filter, and a measured transmittance of 96% for the nonlinear crystal at 790 nm, giving $\tau_{opt} = 87\%$. In addition, we estimate 4% reflectance loss upon exiting fiber and connecting to the detectors coupling lens, and an additional 2% loss due to the four anti-reflection-coated surfaces of the lens L_2, with a final $\tau_{SMF-lens} = 91\%$. The total of these losses, along with the measured raw detection efficiency of $\chi_{\rm D} = 31\%$, implies a mode preparation efficiency of χ_p= 70%. Our setup for practical reasons did not allow for exact spatial mode matching of the heralding and heralded modes (in fact, d_1 and d_2 were different). This is one of the reasons we could not reach the highest predicted efficiency of 86%. As an explanation of the 20% discrepancy between the predicted and measured single mode preparation efficiency, we figure out that, because of the non-perfect longitudinal phase-matching and of the finite transverse pump profile, a single direction in the heralding arm corresponds to an area of correlated photons; this area in a correct calculation is broader and equal in both dimensions, while in our approximation, it results narrower in the y direction. This is because we retain only the first order in the series for the longitudinal mismatch, the remaining transverse contribution is only in the y direction as it is clearly evident from Eq.(6).

5. CW PUMP EXPERIMENTAL SETUP

We have set up (fig. 4) a 5 mm periodically poled lithium niobate (PPLN) crystal pumped by a CW laser at 532 nm to produce 810 nm and 1550 nm photon pairs in a slightly noncollinear geometry. The crystal was operated

in a quasi-phasematching configuration, with noncritical phase-matching (90° phase-matching angle) and a 7.36 μm period to produce PDC photons at 810 nm and 1550 nm at external angles of 1° and 2°. Fine tuning of this output was achieved by adjusting the crystal temperature to 149 °C. A lens, L_p was used in the pump beam to

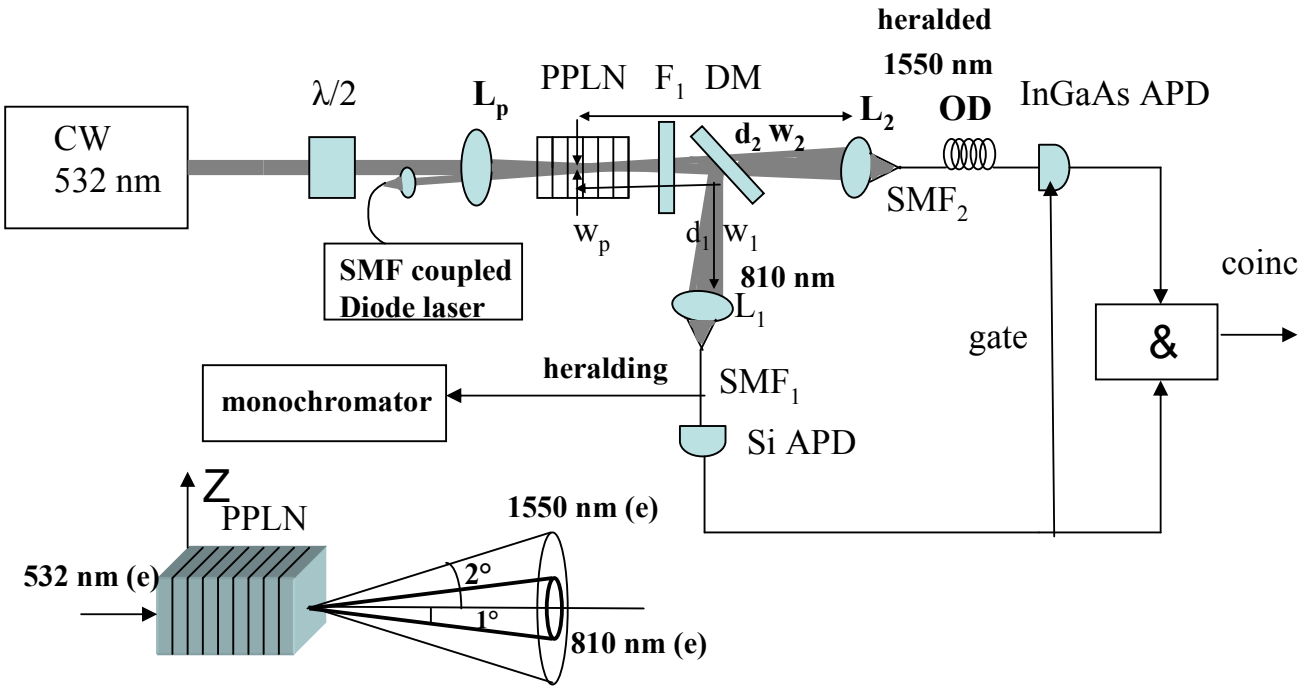

Figure 4. Setup to herald single-photons from CW PDC from a PPLN crystal.

produce a gaussian beam waist of $w_p \simeq 210$ μm at the crystal, a cutoff filter F_1 blocked the pump laser and a dichroic mirror (DM) separated the 810 nm (beam 1) and 1550 nm (beam 2) photons. A monochromator was inserted in the heralding path to align the 810 nm light, measure its spectral width, and as a filter. The heralding arm was routed to a SMF and then to a Si Avalanche Photodiode (APD), while the heralded arm, also coupled to a SMF, was sent to a InGaAs APD, operating in gated mode. The heralded arm optical delay was adjusted with an appropriate length SMF to observe coincidences when the InGaAs detector was gated by the detection of a 810 nm photon in the heralding arm. The InGaAs detector, including the SMF and coupling lens optical losses, was calibrated against a conventional detector standard using a attenuated laser source, yielding a raw detection efficiency of $\eta_{det} = 9.8\%$.

5.1. Experimental results

The mode preparation efficiency as measured by the CW PDC source is given by Eq.(28), where

$$\chi_D = \frac{P_{coinc} - P_{uncorr}}{(1 - P_{uncorr})(1 - P_{backgnd}^{heralding})}, \tag{29}$$

τ_{opt} is the overall heralded arm optical transmittance (including PPLN, F_1, DM), $\tau_{SMF-lens}$ is the optical transmittance of the L_2 and the SMF on the heralded arms, P_{coinc} is the probability of coincident counts per gate, P_{uncorr} is probability of uncorrelated or accidental coincidence counts per gate (determined by changing the heralding delay so the detection gate misses photons correlated to the herald photons), and $P_{backgnd}^{heralding}$ is the probability of gating counts produced by uncorrelated photons and dark counts on the heralding arm. The theoretical mode preparation efficiency is given by Eq.(26), where $\Delta_{1,2}$ =1, 2.7 nm are the spectral bandwidths selected by the SMFs in the two arms.

We used two lens configurations to mode match the fields (refer to Table 2).

With L_1 and L_2 both f=8 mm aspheric lenses, at d_1=270 mm and d_2=220 mm, and $w_1 = w_2$=100 μm, from Eq.(1), we obtained the experimental value of χ_p =64%, while from Eq. (29) we estimate χ_p=61%. With L_1 and L_2 both 20x microscope objectives at d_1=560 mm and d_2=190 mm, and $w_1 = 144\mu$m and w_2=76

Table 2. Details of lens configurations for coupling fiber mode diameter of 4.2 μm and of ?? μm

L_1 @ d_1	$w_{0,1}$ (μm)	M_1	Δ_1 (nm)	$\Delta\theta_1$ (°)	L_2 @ d_2	$w_{0,2}$ (μm)	M_2	Δ_2 (nm)	$\Delta\theta_2$ (°)	χ_p(theory) (%)	χ_p(expt.) (%)
f=8mm	100		1	0.1	f=8mm	100		2.7	0.2	61	64
μ obj., 20x, f=9 mm	144		0.5	0.1	f=8mm	76		3.6	0.3	78	77

μm, we obtained the experimental value of χ_p =77% and the theoretical χ_p=78 %. Those values are in good agreement considering the difficulty to measure the bandwidths and waists at the crystal. The measured values in Eq.(**??**)are P_{coinc}=2.2%, 2.9%, $P_{uncorr}^{heralded}$=0.2 %, 0.3 % and $P_{backgnd}^{heralding}$=41%, 29%. We measured the τ_{opt}=65 % and $\tau_{SMF-lens}$=83 %, 73%, for the lenses and objectives configuration, respectively. The heralding background, properly measured using the monochromator, is due to the fluorescence of the PPLN. In a similar experimental configuration, without the insertion of the monochromator, the InGaAs APD was triggered at 142 KHz, with a 65 mW pump power, yielding 4.2 KHz of coincidences, corresponding to 0.07 pairs/(gate mW) generated. This result is in agreement with the expected efficiency of PPLN for pair production, as reported in.[9]

6. CONCLUSIONS AND FINAL REMARKS

In this paper we analyzed theoretically and experimentally strategies to maximize the heralding efficiency of a PDC pulsed source, considering spatial and spectral mode selection in bulk crystal and of a CW PDC down-converter based on PPLN. We provided a theoretical estimate of the heralding efficiency and of the coincidence spectrum , giving a practical method to tailor heralded photons in a defined spectral and spatial mode. We prove that spatial overlap alone is not enough when we have pulsed pumping and that attention has to be paid to define spectrally the mode preparation efficiency.

The theoretical prediction for this PPLN is in better agreement with the experimental value, because of a better measurement of the heralding bandwidth. This work was supported in part by ARDA, ARO, and DARPA/QUIST.

REFERENCES

1. *Photons and Nonlinear Optics*, D.N. Klyshko, Gordon and Breach Science Publishers (1988).
2. D.C. Burnham and D.L. Weinberg, Phys. Rev. Lett. **25**, 84 (1970).
3. Migdall A L, Castelletto S, Degiovanni I P, and Rastello M L *Appl. Opt.*, vol. 41, pp. 2914-,2002
4. Tittel W, Brendel J, Zbinden H and Gisin N *Phys. Rev. Lett.* vol. 84, 4737-, 2000
5. E. Knill, R. Laflamme, and G.J. Milburn, Nature **409**, 46 (2001).
6. D. Bouwmeester *et.al.*, Nature **390**, 575 (1997);
7. A.I. Lvovsky *et.al.*, Phys. Rev. Lett. **87**, 050402 (2001).
8. S. Castelletto, I.P. Degiovanni,V. Schettini, M. Ware, and A. Migdall, Proceedings of the "*Quantum Communications and Quantum Imaging*", (AM112), paper 5551-13, Part of SPIE's International Symposium on Optical Science and Technology, SPIE's 49th Annual Meeting 2-6 August 2004, Denver, CO, USA
9. M. A. Albota et al., J. of Modern Physics, **51**, 1417-1432(2004)
10. F.A. Bovino *et.al.*, Opt. Comm. **227**, 343 (2003).
11. T.B. Pittmann, B. C. Jacobs, and J.D. Franson quant-ph/0408093, also accepted for pubblication in Optics Communication.
12. S. Castelletto et al., submitted to Optics Express.
13. A. Dragan, quant-ph/0407113.
14. S. Castelletto, I.P. Degiovanni, M. Ware, and A. Migdall, "*New Journal of Physics*",vol.6, n.87 (2004).
15. Rubin M H *Phys. Rev. A*, vol. 54, pp. 5349, 1996
16. We calibrated the detector efficiency by using a mulitmode fiber in the same configuration of coupling lenses used with the SMF after testing that in the heralded arm the correlated photons were collected.